

Numerical analysis of voltage-controlled magnetization switching operation in magnetic-topological-insulator-based devices

Takashi Komine^{1, a)} and Takahiro Chiba^{2, 3}

¹⁾ Graduate School of Science and Engineering, Ibaraki University, 4-12-1, Nakanarusawa, Hitachi, Ibaraki, 316-8511, Japan

²⁾ Frontier research Institute for Interdisciplinary Sciences, Tohoku University, Sendai, Miyagi 980-0845, Japan

³⁾ Department of Applied Physics, Graduate School of Engineering, Tohoku University, Sendai, Miyagi 980-8579, Japan

(Dated: 7 September 2023)

We theoretically investigate influences of electronic circuit delay, noise and temperature on write-error-rate (WER) in voltage-controlled magnetization switching operation of a magnetic-topological-insulator-based (MTI) device by means of the micromagnetic simulation. This device realizes magnetization switching via spin-orbit torque (SOT) and voltage-controlled magnetic anisotropy (VCMA) which originate from 2D-Dirac electronic structure. We reveal that the device operation is extremely robust against circuit delay and signal-to-noise ratio. We demonstrate that the WER on the order of approximately 10^{-4} or below is achieved around room temperature due to steep change in VCMA. Also, we show that the larger SOT improves thermal stability factor. This study provides a next perspective for developing voltage-driven spintronic devices with ultra-low power consumption.

Electrical control of magnetization has attracted much attention for next generation spintronic devices such as non-volatile magnetic memory¹, high-speed logic², and low-power data transmission³. Voltage-controlled magnetization anisotropy (VCMA) is a promising way to drive magnetization switching with high energy efficiency, and to realize magnetic memories and logic devices with low power consumption⁴⁻⁹. Although VCMA is expected to have superior energy efficiency, the VCMA-driven magnetization switching faces practical issues including the write-error rate (WER), narrow operating window, and necessity for external bias magnetic field¹⁰. The reduction of WER in VCMA-driven magnetic devices is especially a serious issue for the practical applications^{11,12}.

While the voltage-control of ferromagnetic metal/non-magnetic insulator bilayers, such as CoFe/MgO, is commonly studied, a perpendicular voltage also shifts the Fermi energy of Dirac electrons on the surface of magnetic topological insulator (MTI). Three-dimensional topological insulators (TIs), such as Bi₂Se₃, have an insulating bulk and conducting surface states¹³. MTIs are ferromagnetically ordered by injection of magnetic dopants into TIs¹⁴. Recently, the electric field effect in a magnetic topological insulator (MTI) and a TI/ferromagnetic insulator bilayer has been investigated by both theoretical and experimental studies¹⁵⁻¹⁸. On the other hand, current-induced spin-orbit torque (SOT) on TI is another key method of manipulating magnetic moment^{18,19}, enabling a deterministic magnetization switching without external magnetic field²⁰⁻²². Furthermore, engineering the SOT efficiency by means of a

voltage (or an electric-field) is a crucial method for practical device applications^{20,23}. Hence, it is highly desirable to simultaneously control the magnetic anisotropy and SOT by a voltage in MTI-based devices for high energy efficiency.

Recently, Chiba *et al.* proposed the field-effect-transistor (FET)-like devices which consists of TI and MTI²⁴⁻²⁶. They presented two distinct methods for the magnetization switching by using electric field control of SOT and perpendicular magnetic anisotropy in TI and MTI hybrid systems. It was reported clear magnetization switching by combining adequate source-drain voltage and gate pulse. The writing energy of $< 0.1\text{fJ/bit}$ is expected for the practical use of voltage-induced magnetization switching devices. The power consumption of the MTI device can be achieved about 1fJ/bit , which is sufficiently reduced. Although the gate pulse shape and the signal-to-noise ratio affect the WER by peripheral electrical circuits in the practical application, WER in the MTI device has not been discussed yet. In this study, we demonstrate magnetization switching in the MTI devices under external disturbance such as electrical circuit noise and thermal fluctuation by the micromagnetic simulation.

Figure 1 illustrates a MTI-based device involving a MTI film as in which the top of the surface of MTI is a conduction-channel layer. By applying a source-drain electric field \mathbf{E}_{sd} and gate voltage V_g , this device realizes magnetization switching via SOT and VCMA without external bias magnetic field. In this device, the anomalous Hall effect is used for readout.

In order to analyze the detail operation and WER of the MTI-based device, the macro-spin model based on the following Landau-Lifshitz-Gilbert (LLG) equation was utilized:

$$\dot{\mathbf{m}} = -\gamma \mathbf{m} \times \mathbf{B}_{\text{eff}} + \alpha \mathbf{m} \times \dot{\mathbf{m}} + \mathbf{T}_{\text{SO}}(E_{\text{sd}}, V_g), \quad (1)$$

^{a)} Electronic mail: takashi.komine.nfm@vc.ibaraki.ac.jp

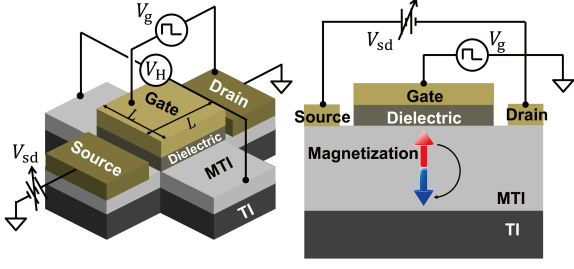


FIG. 1. Schematic illustration of a MTI-based device with a FET-like structure consisting of magnetic-TI (MTI) and TI film.

where γ is the gyromagnetic constant, α the Gilbert damping parameter, and the effective field \mathbf{B}_{eff} includes

$$\mathbf{B}_{\text{eff}} = \mathbf{B}_d + \mathbf{B}_k(V_g) + \mathbf{B}_{\text{th}}(T). \quad (2)$$

where \mathbf{B}_d , \mathbf{B}_k and \mathbf{B}_{th} are the demagnetizing field, the anisotropy field, and the thermal fluctuation field, respectively. The anisotropy field \mathbf{B}_k is tunable by the gate voltage V_g or the corresponding Fermi level E_F . Here, the SOT \mathbf{T}_{SO} depends on the gate voltage V_g and source-drain electric field E_{sd} , which are derived from 2D-Dirac electronic structure at the interface between the dielectric and MTI film²⁵. Moreover, the thermal fluctuation field \mathbf{B}_{th} with 3D Gaussian distribution of dispersion is taken into account.

$$\sigma^2 = \frac{2\alpha k_B T}{\gamma M_s (1 + \alpha^2) V \Delta t}, \quad (3)$$

The SOT term \mathbf{T}_{SO} depends on the source-drain electric field E_{sd} and the gate voltage V_g as follow:

$$\mathbf{T}_{\text{SO}}(E_{\text{sd}}, V_g) = -\frac{\gamma \Delta}{M_s d} \mathbf{m} \times \boldsymbol{\mu}(E_{\text{sd}}, V_g) \equiv -\gamma \mathbf{m} \times \mathbf{B}_{\text{SOT}}, \quad (4)$$

where $\boldsymbol{\mu}$ is the electrically induced nonequilibrium spin polarization, and Δ is the spin splitting of 2D-Dirac electrons or the exchange interaction coupled to the homogeneous localized moment of MTI. This term acts the effective fields along the longitudinal component μ_x and the transverse component μ_y as functions of E_{sd} and V_g as follows

$$\boldsymbol{\mu}(E_{\text{sd}}, V_g) = \mu_x(E_{\text{sd}}, V_g) \hat{\mathbf{x}} + \mu_y(E_{\text{sd}}, V_g) \hat{\mathbf{y}}, \quad (5)$$

$$\mu_x(E_{\text{sd}}, V_g) = \frac{4eE_{\text{sd}} \Delta}{\hbar v_F} \frac{E_F(V_g) m_z [E_F^2(V_g) + \Delta^2 m_z^2]}{[E_F^2(V_g) + 3\Delta^2 m_z^2]^2} \quad (6)$$

$$\mu_y(E_{\text{sd}}, V_g) = \frac{eE_{\text{sd}}}{2\hbar v_F} \frac{E_F(V_g) \tau}{\hbar} \frac{E_F^2(V_g) - \Delta^2 m_z^2}{E_F^2(V_g) + 3\Delta^2 m_z^2}. \quad (7)$$

Note that the estimated domain size and the domain wall width are about 400 nm and 150 nm, respectively. The uniform domain appears in the MTI-based device consisting of uniform materials when the device size is less

TABLE I. Material parameters.

Gilbert damping, α	0.1
Surface gap in Dirac cone, 2Δ (meV) ^{14,41,42}	60
Bulk band gap, $2\Delta_c$ (meV)	200
Fermi velocity in Dirac cone, v_F (m s ⁻¹)	4×10^5
Dielectric constant in TI, ϵ_r	9.7
Saturation magnetization, M_s (kA m ⁻¹) ⁴³	8.5
TI thickness, d_{TI} (nm)	7
Dielectric thicknesses, d_D (nm)	20

than 1 μ m, and the magnetization switching occurs corresponding to rotation mode under the application of gate voltage and source-drain electric field. Thus, the macro-spin model is valid for analysis of magnetization switching behavior and WER.

In magnetic tunnel junction (MTJ) devices, the VCMA as a function of pulse voltage V_{pulse} is a odd function due to charge accumulation at the magnetic layer²⁷⁻³⁰. The VCMA coefficient ξ in the MTI device approximately reaches -350 fJ/Vm estimated as defined $\xi = (\delta K_u t) / \delta E_{\text{pulse}}$ by the same manner of MTJ¹⁰. On the other hand, in the MTI-based devices, the VCMA as a function of gate pulse voltage V_g is an even function due to the Fermi level tuning in the gap-opened Dirac dispersion. By the same manner, the VCMA coefficient is about -4 fJ/Vm but the anisotropy K_u reaches to zero at the gate voltage of 0.4 V. In the MTI-based device, comparably small gate voltage can control the maximum to the minimum in the Dirac magnetic anisotropy K_u .

In MTJ, the VCMA effect has been used to assist the magnetization switching in combination with an external field³¹⁻³³, the spin-transfer-torque³⁴, the crystallographic strain³⁵, thermally excitation³⁶, or the SOT³⁷⁻⁴⁰ to reduce the write energy. In the MTI-based device, the SOTs including both field-like and damping-like terms assists the VCMA magnetization switching by applying the source-drain electric field E_{sd} .

Although in the previous report, the ideal square wave of gate pulse with pulse duration τ_g are applied for magnetization switching, the practical pulse has the electronic circuit delay and electrical noise. In this study, the 1st-order filter with cut-off frequency f_c ,

$$G(f) = \frac{1}{1 + j \frac{f}{f_c}}, \quad (8)$$

was used as the circuit delay, and the cut-off dependence of WER was investigated. The device has dimensions of $L \times L \times 7$ nm, and the length L is 1 μ m as the standard size in the simulation. The material parameters related to MTI-based system are listed in Table I.

At the beginning, we demonstrate magnetization reversal in the MTI-based device under the circumstance with typical circuit and thermal noises. In the MTI-based device, the VCMA is a trigger to switch the magnetization direction while the SOT induces magnetization switching trajectory, *i.e.*, the SOT due to source-drain electric field

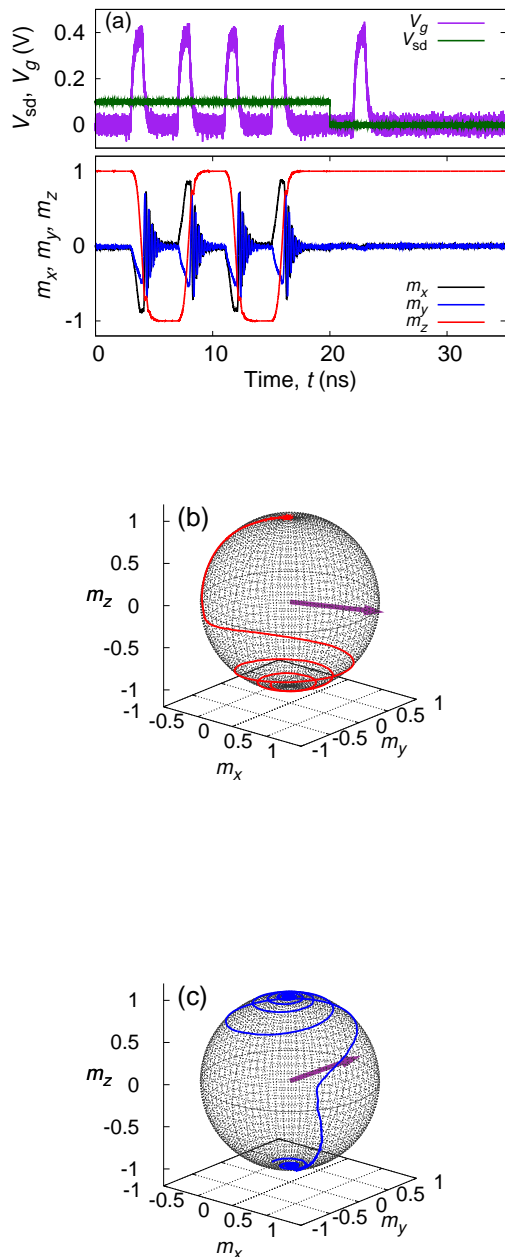


FIG. 2. (a) Magnetization switching behavior under the application of source-drain electric field E_{sd} of $1 \times 10^5 \text{ V m}^{-1}$ and gate pulse with the duration τ_g of 1 ns and the gate voltage V_g of 0.39 V. The gate pulse is passed through the 1st-order filter with f_c of 5 GHz, the SNRs for both gate and source-drain voltages are 27 dB, and the temperature T is set to 300 K. Corresponding magnetization trajectories of (b) changing from upward to downward and (c) changing from upward to downward. The purple arrow indicate an effective magnetic field due to the spin-orbit torque.

takes a role of an external magnetic field in VCMA-MTJ devices.

Figure 2 shows magnetization switching behavior under the application of source-drain and gate voltages. When the gate voltage V_g of 0.39 V is applied, the magnetic anisotropy sharply goes down to zero, enabling the magnetization to be along an arbitrary direction (see also Supplementary material). Hence, during the duration of V_g the SOT due to E_{sd} derives to magnetization reversal. On the other hand, when V_{sd} is not applied, the magnetization is not reversed even if the gate pulse is applied. Corresponding energy distribution as a function of azimuth angle and z -component of magnetization are shown in the Supplementary material. Such a feature of this device is that magnetization reversal occurs by applying an appropriate gate pulse regardless of the polarity of the magnetization from upward to downward or from downward to upward.

Figure 3(a) shows the switching probability P_{sw} as a function of gate pulse duration τ_g and source-drain electric field E_{sd} . The switching probability $P_{sw} = N_{sw}/N_{tot}$ was calculated from the number of successful switchings, N_{sw} , against a million of gate voltage inputs, N_{tot} , without electrical noise under thermal fluctuation of 300 K. Clearly, the switching probability oscillates depending on both τ_g and E_{sd} . Consequently, switching will be achieved in the wide pulse duration. The magnetization switching occurs due to characteristic frequency determined by SOT or E_{sd} . Thus, the adequate pulse duration τ_g is determined by SOT strength, and, in any case, the pulse duration τ_g and the source-drain electric field E_{sd} provide wide operation window. The operation window can be estimated as follows:

$$\tau_g = \frac{(2n+1)\pi(1-\alpha^2)}{\gamma B_{SOT}}, \quad (n = 0, 1, 2, \dots), \quad (9)$$

which means the source-drain electric field can manipulate the operation window or the desired pulse duration. Figures 3(b)-(d) also show the switching probability P_{sw} as a function of gate pulse duration τ_g and gate voltage V_g . Clearly, the switching probability oscillates depending on only the gate pulse width when the gate voltage is larger than 0.39 V vanishing magnetic anisotropy. The operation window period decreases as the SOT strength increases according to Eq.(9). On the other hand, when the gate voltage is smaller than 0.39 V, the distorted operation windows were observed due to the SOT. The gate voltage which enables the magnetization switching becomes smaller as the SOT strength increases. These results are in good agreements with the estimated operation windows. For parameter set (1) as shown in Fig.3, the source-drain electric field of 0.1 MV m^{-1} is equivalent to the B_{SOT} magnitude of about 12 mT. The corresponding operation window τ_g is about 1.4 ns, which is moderately high-speed and is easy to handle the write operation by the present CMOS technology. In order to investigate WERs, three pairs of appropriate parameters of τ_g and E_{sd} were chosen as shown in Fig.3(a). The

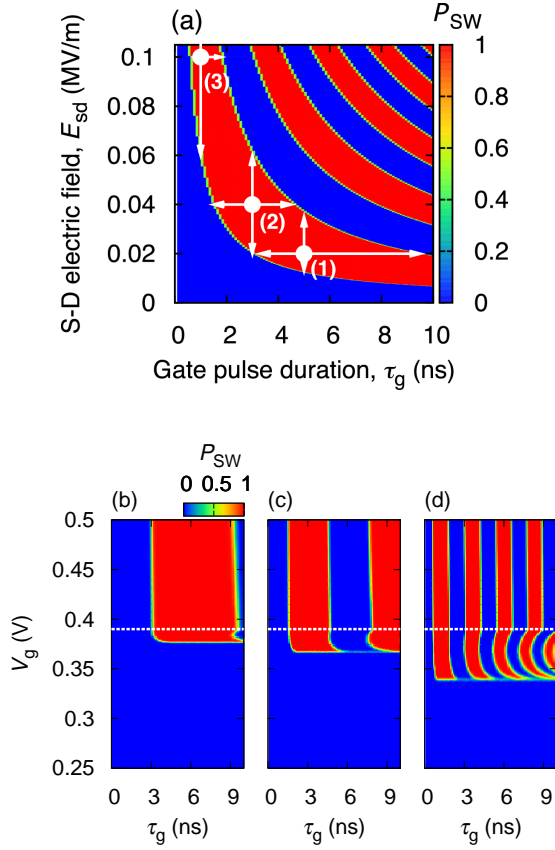


FIG. 3. (a) Switching probability P_{SW} as a function of source-drain electric field E_{sd} and gate pulse duration τ_g with ideal square pulse. The gate voltage is set to 0.39 V. The Gilbert damping α is set to 0.1 and the temperature T is set to 300 K. Magnetization switching probabilities as a function of gate voltage V_g and gate pulse duration τ_g with ideal square pulse. The temperature T is set to 300 K. Figures (b), (c), and (d) correspond to the parameter sets (1), (2), and (3) shown in (a), respectively.

WERs, $1 - N_{sw}/N_{tot}$, were also calculated from the number of failure switching or write-error for various cut-off frequencies without the other fluctuation.

In order to investigate the electric circuit delay, the cut-off frequency f_c for gate pulse was varied and calculated WER. Figure 4 (a) shows cut-off frequency dependence of WER. Since the adequate gate pulse τ_g becomes shorter as E_{sd} becomes larger, the required f_c must be higher. Since the rise time τ_c for 1st-order filter is defined to be $1/f_c$, the ratio $1 - \tau_c/\tau_g$ expresses the effective induction ratio of VCMA as shown in Fig.4 (b). If the rise time is about 15% smaller than the gate pulse width, the excellent WER can be obtained in each gate pulse. The appropriate gate pulse can be chosen from the cut-off frequency in the practical electric circuit.

We also investigated the SNR dependence of WER for source-drain electric field E_{sd} . The source-drain electric field E_{sd} is immune to noise, and the required SNR is as very low as -20 dB. Figure 4 (c) shows WER as a

TABLE II. Thermal stability estimated from calculated WERs as shown in Fig.4(d). The device size L of 100 nm was used in these results.

Source-drain field E_{sd} [MV m ⁻¹]	Thermal stability $K_u V/k_B T$ ($T = 300$ K)
0.02	4.3
0.04	14.7
0.1	20.3
0.1, ($\alpha = 0.01$)	40.2

function of SNR against the gate voltage V_g . For larger E_{sd} which corresponds to long pulse duration τ_g , the required SNR of gate voltage becomes larger because of the SOT assist by the source-drain electric field E_{sd} . Both required cut-off frequency and SNRs can be sufficiently implemented in the practical application of this device. Thus, the MTI-based device is extremely robust against circuit delay and signal-to-noise ratio.

Alike the voltage-controlled MTJ, the thermal fluctuation of magnetization also gives rise an unexpected effect on the device operation. Since the thermal fluctuation effect on WER becomes more prominent as the device size becomes smaller. Thus, the device size is set to 100 nm in the simulation. Figure 5 shows the temperature dependence of WER in three different types of operation as shown in Fig.3. Three type operations have different thermal stability factors. As the larger SOT induces, the thermal stability factor improves more. In the type (3) operation as shown in Fig.3, the gate pulse duration is 1 ns and high speed operation is a promising. By fitting the slope of WER, the estimated thermal stability factors $K_u V/k_B T$ are shown in TableII. The estimated thermal stability factors $K_u V/k_B T$ is more than 40 in the device size of 100 nm and smaller damping constant α , which are sufficient for the practical application. The SOT plays a role of the external magnetic field which is similar to the external magnetic field in the VCMA-MTJ device. The effective anisotropy field, $B_k^* = \sqrt{B_k^2 + B_{SOT}^2}$, can be estimated, where B_k and B_{SOT} are the intrinsic anisotropy field and the field strength corresponding to the SOT. Thus, the thermal stability is enhanced during the application of SOT as the SOT increases.

As the above-mentioned, the VCMA-MTI device has a feasible feature of VCMA and superior WER characteristics comparing with VCMA-MTJ. Furthermore, the writing energy of VCMA-MTI is less than that of VCMA-MTJ due to steep change in VCMA of MTI. On the other hand, the Curie temperature and thermal stability of MTI are much less than that of materials in the MTJ device. Since the thermal stability is related to the magnetically-opened bandgap in MTI, development of potential materials is important to realize the proposed MTI-based device. Finally, we briefly mention about potential materials to fabricate the MTI-based device. To realize MTIs, most of the past research has been dedicated to Cr-doped TI, which restricts the Curie temperature to be around 10-20 K^{44,45}. For practical device

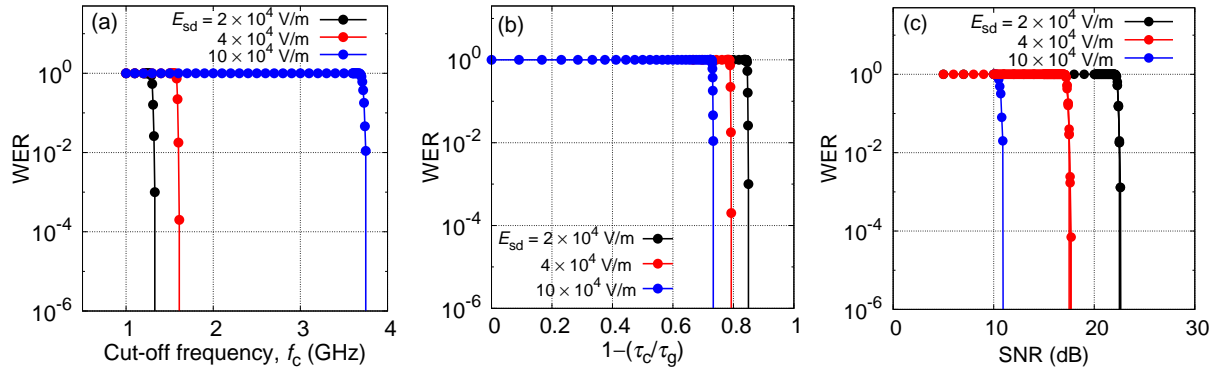


FIG. 4. (a) WER as a function of cut-off frequency f_c , and (b) WER as a function of $1 - \tau_c/\tau_g$ which corresponds to the effective induction ratio of VCMA. (c) WER as a function of signal-to-noise ratio (SNR).

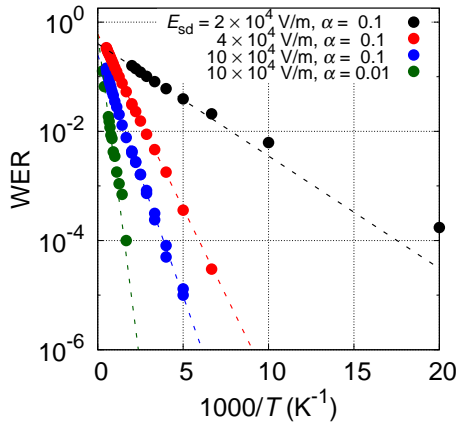


FIG. 5. Write-error-rate (WER) as a function of temperature T . The device size L of 100 nm was used.

applications, room-temperature MTIs would be essential and resent intensive studies for MTIs with other magnetic dopants will facilitate the realization of the presented device.

In summary, we theoretically investigate influences of electronic circuit delay, noise and temperature on write-error-rate (WER) in voltage-controlled magnetization switching operation of a MTI-based device by means of the micromagnetic simulation. This device realizes magnetization switching via SOT and VCMA which originate from 2D-Dirac electronic structure. We reveal that the device operation is extremely robust against circuit delay and SNR. We demonstrate that the WER on the order of approximately 10^{-4} or below is achieved around room temperature due to steep change in VCMA. Also, we show that the larger SOT improves thermal stability factor. Therefore, this study provides a next perspective for developing voltage-driven spintronic devices with ultra-low power consumption.

SUPPLEMENTARY MATERIAL

See the supplementary material for the energy surface, trajectory, and fully micromagnetic understanding during magnetization switching.

This work was partly supported by Grants-in-Aid for Scientific Research (Grants No. 20H02196, 22K14591, 22H01805, 20K03814, 18KK0132) from the Japan Society for the Promotion of Science, by the Spintronics Research Network of Japan (Spin-RNJ). This work was partially performed under the Research Program of “Dynamic Alliance for Open Innovation Bridging Human, Environment and Materials” in “Network Joint Research Center for Materials and Devices”.

¹K. Ando, S. Fujita, J. Ito, S. Yuasa, Y. Suzuki, Y. Nakatani, T. Miyazaki, and H. Yoda, *Journal of Applied Physics* **115** (2014), 10.1063/1.4869828.

²P. Barla, V. K. Joshi, and S. Bhat, *J. Comp. Electron.* **20**, 805 (2021).

³Y. Zhang, W. Zhao, J.-O. Klein, W. Kang, D. Querlioz, Y. Zhang, D. Ravelosona, and C. Chappert, in *2014 Design, Automation & Test in Europe Conference & Exhibition (DATE)* (2014) pp. 1–6.

⁴T. Maruyama, Y. Shiota, T. Nozaki, K. Ohta, N. Toda, M. Mizuguchi, A. A. Tulapurkar, T. Shinjo, M. Shiraishi, S. Mizukami, Y. Ando, and Y. Suzuki, *Nat. Nanotech.* **4**, 158–161 (2009).

⁵M. Endo, S. Kanai, S. Ikeda, F. Matsukura, and H. Ohno, *Appl. Phys. Lett.* **96**, 212503 (2010).

⁶Y. Shiota, T. Nozaki, F. Bonell, S. Murakami, T. Shinjo, and Y. Suzuki, *Nat. Mater.* **11**, 39 (2011).

⁷Y. Shiota, S. Miwa, T. Nozaki, F. Bonell, N. Mizuochi, T. Shinjo, H. Kubota, S. Yuasa, and Y. Suzuki, *Appl. Phys. Lett.* **101**, 102406 (2012).

⁸Y. Shiota, T. Nozaki, S. Tamaru, K. Yakushiji, H. Kubota, A. Fukushima, S. Yuasa, and Y. Suzuki, *Appl. Phys. Express* **9**, 013001 (2015).

⁹C. Grezes, F. Ebrahimi, J. G. Alzate, X. Cai, J. A. Katine, J. Langer, B. Ocker, P. Khalili Amiri, and K. L. Wang, *Appl. Phys. Lett.* **108**, 012403 (2016).

¹⁰T. Yamamoto, R. Matsumoto, T. Nozaki, H. Imamura, and S. Yuasa, *J. Magn. Magn. Mater.* **560**, 169637 (2022).

¹¹Y. Shiota, T. Nozaki, S. Tamaru, K. Yakushiji,

- H. Kubota, A. Fukushima, S. Yuasa, and Y. Suzuki, *Appl. Phys. Lett.* **111**, 022408 (2017).
- ¹²T. Yamamoto, T. Nozaki, H. Imamura, Y. Shiota, T. Ikeura, S. Tamaru, K. Yakushiji, H. Kubota, A. Fukushima, Y. Suzuki, and S. Yuasa, *Phys. Rev. Appl.* **11**, 014013 (2019).
- ¹³Y. Ando, *J. Phys. Soc. Jpn.* **82**, 102001 (2013).
- ¹⁴Y. Tokura, K. Yasuda, and A. Tsukazaki, *Nat. Rev. Phys.* **1**, 126 (2019).
- ¹⁵J. Wang, B. Lian, and S.-C. Zhang, *Phys. Rev. Lett.* **115**, 036805 (2015).
- ¹⁶A. Sekine and T. Chiba, *Phys. Rev. B* **93**, 220403 (2016).
- ¹⁷Y. G. Semenov, X. Duan, and K. W. Kim, *Phys. Rev. B* **86**, 161406 (2012).
- ¹⁸Y. Fan, X. Kou, P. Upadhyaya, Q. Shao, L. Pan, M. Lang, X. Che, J. Tang, M. Montazeri, K. Murata, L.-T. Chang, M. Akyol, G. Yu, T. Nie, K. L. Wong, J. Liu, Y. Wang, Y. Tserkovnyak, and K. L. Wang, *Nat. Nanotech.* **11**, 352 (2016).
- ¹⁹N. H. D. Khang, Y. Ueda, and P. N. Hai, *Nat. Mater.* **17**, 808 (2018).
- ²⁰K. Cai, M. Yang, H. Ju, S. Wang, Y. Ji, B. Li, K. W. Edmonds, Y. Sheng, B. Zhang, N. Zhang, S. Liu, H. Zheng, and K. Wang, *Nat. Mater.* **16**, 712 (2017).
- ²¹Y. Cao, Y. Sheng, K. W. Edmonds, Y. Ji, H. Zheng, and K. Wang, *Adv. Mater.* **32**, 1907929 (2020).
- ²²Z. A. Bekele, X. Liu, Y. Cao, and K. Wang, *Adv. Electron. Mater.* **7**, 2000793 (2021).
- ²³M. Filianina, J.-P. Hanke, K. Lee, D.-S. Han, S. Jaiswal, A. Rajan, G. Jakob, Y. Mokrousov, and M. Kläui, *Phys. Rev. Lett.* **124**, 217701 (2020).
- ²⁴T. Chiba, S. Takahashi, and G. E. W. Bauer, *Phys. Rev. B* **95**, 094428 (2017).
- ²⁵T. Chiba and T. Komine, *Phys. Rev. Appl.* **14**, 034031 (2020).
- ²⁶T. Chiba, A. O. Leon, and T. Komine, *Appl. Phys. Lett.* **118**, 252402 (2021).
- ²⁷M. Weisheit, S. Fähler, A. Marty, Y. Souche, C. Poinignon, and D. Givord, *Science* **315**, 349 (2007).
- ²⁸M. Tsujikawa and T. Oda, *Phys. Rev. Lett.* **102**, 247203 (2009).
- ²⁹K. Nakamura, R. Shimabukuro, Y. Fujiwara, T. Akiyama, T. Ito, and A. J. Freeman, *Phys. Rev. Lett.* **102**, 187201 (2009).
- ³⁰C.-G. Duan, J. P. Velev, R. F. Sabirianov, Z. Zhu, J. Chu, S. S. Jaswal, and E. Y. Tsybal, *Phys. Rev. Lett.* **101**, 137201 (2008).
- ³¹Y. Shiota, T. Maruyama, T. Nozaki, T. Shinjo, M. Shiraishi, and Y. Suzuki, *Appl. Phys. Express* **2**, 063001 (2009).
- ³²P. Khalili Amiri, P. Upadhyaya, J. G. Alzate, and K. L. Wang, *J. Appl. Phys.* **113**, 013912 (2013).
- ³³G. Han, H. Meng, J. Huang, V. Naik, C. Sim, M. Tran, and T. Lim, *IEEE Trans. Magn.* **51**, 1 (2015).
- ³⁴S. Kanai, Y. Nakatani, M. Yamanouchi, S. Ikeda, H. Sato, F. Matsukura, and H. Ohno, *Appl. Phys. Lett.* **104**, 212406 (2014).
- ³⁵Y. Kato, H. Yoda, Y. Saito, S. Oikawa, K. Fujii, M. Yoshiki, K. Koi, H. Sugiyama, M. Ishikawa, T. Inokuchi, N. Shimomura, M. Shimizu, S. Shirotori, B. Altansargai, Y. Ohsawa, K. Ikegami, A. Tiwari, and A. Kurobe, *Appl. Phys. Express* **11**, 053007 (2018).
- ³⁶T. Yamamoto, T. Nozaki, Y. Shiota, H. Imamura, S. Tamaru, K. Yakushiji, H. Kubota, A. Fukushima, Y. Suzuki, and S. Yuasa, *Phys. Rev. Appl.* **10**, 024004 (2018).
- ³⁷H. Yoda, N. Shimomura, Y. Ohsawa, S. Shirotori, Y. Kato, T. Inokuchi, Y. Kamiguchi, B. Altansargai, Y. Saito, K. Koi, H. Sugiyama, S. Oikawa, M. Shimizu, M. Ishikawa, K. Ikegami, and A. Kurobe, in *2016 IEEE International Electron Devices Meeting (IEDM)* (2016) pp. 27.6.1–27.6.4.
- ³⁸T. Inokuchi, H. Yoda, Y. Kato, M. Shimizu, S. Shirotori, N. Shimomura, K. Koi, Y. Kamiguchi, H. Sugiyama, S. Oikawa, K. Ikegami, M. Ishikawa, B. Altansargai, A. Tiwari, Y. Ohsawa, Y. Saito, and A. Kurobe, *Appl. Phys. Lett.* **110**, 252404 (2017).
- ³⁹S.-h. C. Baek, K.-W. Park, D.-S. Kil, Y. Jang, J. Park, K.-J. Lee, and B.-G. Park, *Nat. Electron.* **1**, 398 (2018).
- ⁴⁰R. Mishra, F. Mahfouzi, D. Kumar, K. Cai, M. Chen, X. Qiu, N. Kioussis, and H. Yang, *Nat. Commun.* **10**, 248 (2019).
- ⁴¹T. Hirahara, S. V. Eremeev, T. Shirasawa, Y. Okuyama, T. Kubo, R. Nakanishi, R. Akiyama, A. Takayama, T. Hajiri, S.-i. Ideta, M. Matsunami, K. Sumida, K. Miyamoto, Y. Takagi, K. Tanaka, T. Okuda, T. Yokoyama, S.-i. Kimura, S. Hasegawa, and E. V. Chulkov, *Nano Letters* **17**, 3493 (2017).
- ⁴²M. Mogi, T. Nakajima, V. Ukleev, A. Tsukazaki, R. Yoshimi, M. Kawamura, K. S. Takahashi, T. Hanashima, K. Kakurai, T.-h. Arima, M. Kawasaki, and Y. Tokura, *Phys. Rev. Lett.* **123**, 016804 (2019).
- ⁴³Y. Fan, X. Kou, P. Upadhyaya, Q. Shao, L. Pan, M. Lang, X. Che, J. Tang, M. Montazeri, K. Murata, L.-T. Chang, M. Akyol, G. Yu, T. Nie, K. L. Wong, J. Liu, Y. Wang, Y. Tserkovnyak, and K. L. Wang, *Nat. Nanotech.* **11**, 352 (2016).
- ⁴⁴B. Li, Q. Fan, F. Ji, Z. Liu, H. Pan, and S. Qiao, *Phys. Lett. A* **377**, 1925 (2013).
- ⁴⁵C.-Z. Chang, J. Zhang, M. Liu, Z. Zhang, X. Feng, K. Li, L.-L. Wang, X. Chen, X. Dai, Z. Fang, X.-L. Qi, S.-C. Zhang, Y. Wang, K. He, X.-C. Ma, and Q.-K. Xue, *Adv. Mater.* **25**, 1065 (2013).